Volume 17
Number 3
21 January 2021
Pages 413–772

# Soft Matter

rsc.li/soft-matter-journal

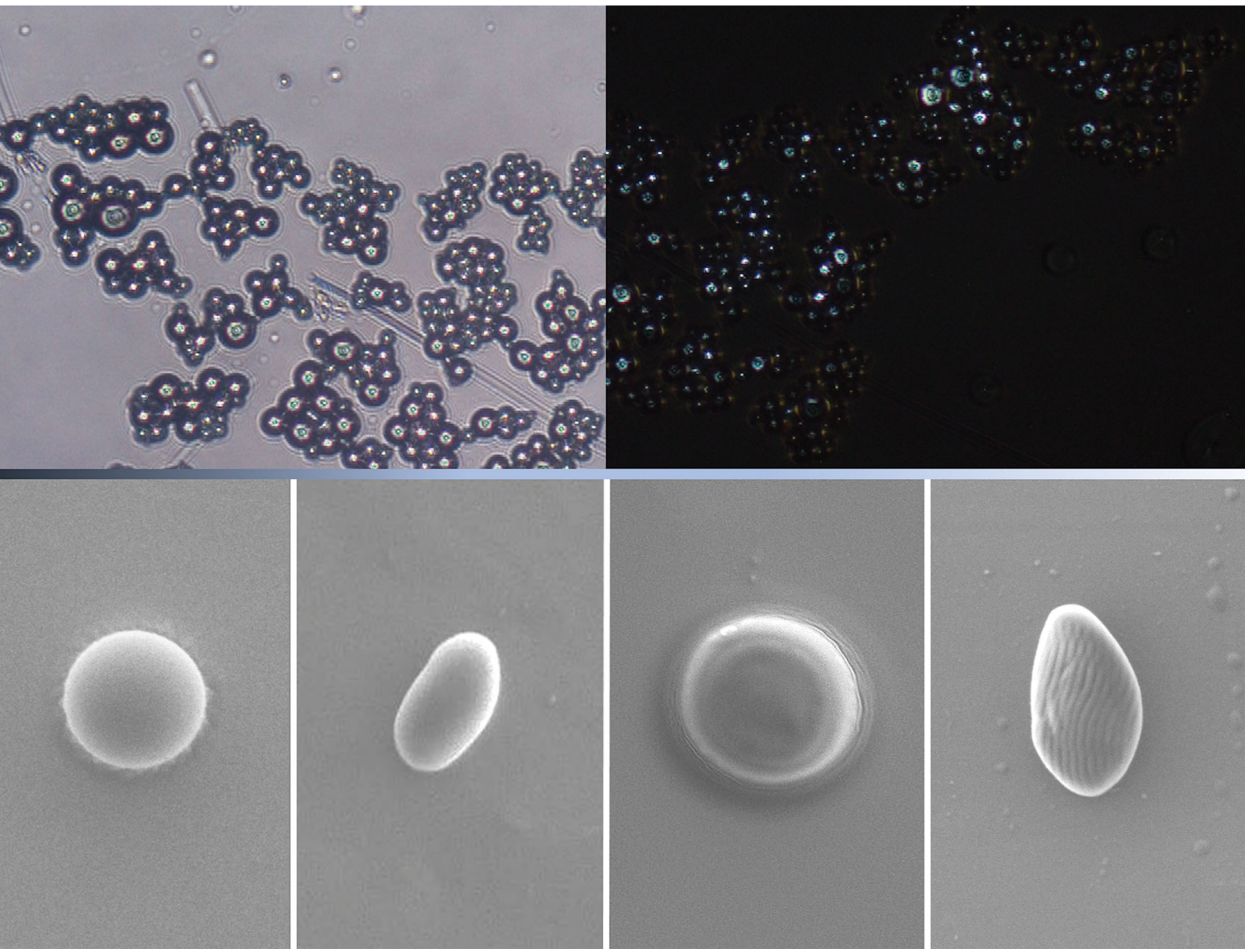

ISSN 1744-6848

ROYAL SOCIETY OF CHEMISTRY

**COMMUNICATION**
Alina M. Martinez *et al.*
Permanent and reversibly programmable shapes in liquid crystal elastomer microparticles capable of shape switching

Soft Matter

COMMUNICATION

View Article Online
View Journal | View Issue





Cite this: *Soft Matter*, 2021, **17**, 467

Received 14th October 2020,
Accepted 8th December 2020

DOI: 10.1039/d0sm01836h

rsc.li/soft-matter-journal

# Permanent and reversibly programmable shapes in liquid crystal elastomer microparticles capable of shape switching†

Alina M. Martinez,[a] Lewis M. Cox,[b] Jason P. Killgore,[c] Nicholas J. Bongiardina,[a] Russell D. Riley[d] and Christopher N. Bowman *[ad]

**Reversibly programmable liquid crystal elastomer microparticles (LCEMPs), formed as a covalent adaptable network (CAN), with an average diameter of 7 μm ± 2 μm, were synthesized *via* a thiol-Michael dispersion polymerization. The particles were programmed to a prolate shape *via* a photoinitiated addition–fragmentation chain-transfer (AFT) exchange reaction by activating the AFT after undergoing compression. Due to the thermotropic nature of the AFT-LCEMPs, shape switching was driven by heating the particles above their nematic–isotropic phase transition temperature ($T_{NI}$). The programmed particles subsequently displayed cyclable two-way shape switching from prolate to spherical when at low or high temperatures, respectively. Furthermore, the shape programming is reversible, and a second programming step was done to erase the prolate shape by initiating AFT at high temperature while the particles were in their spherical shape. Upon cooling, the particles remained spherical until additional programming steps were taken. Particles were also programmed to maintain a permanent oblate shape. Additionally, the particle surface was programmed with a diffraction grating, demonstrating programmable complex surface topography *via* AFT activation.**

Microparticles have been the subject of significant research efforts due their incorporation into a wide range of applications including cosmetics, drug therapy, optics, and adsorption, amongst others.[1–5] Numerous methodologies exist for generating microparticles and a key objective in related research has been overcoming the static nature of microparticle geometry. Shape changing microparticles are of growing interest since dynamic control over geometry facilitates integration into a wider range of applications demanding optical dynamics, tunable adhesion, rheological control, and micromechanical actuation.[6–9]

Beyond typical one-way shape switching phenomena, two-way shape switching materials are desirable for their inherent ability to change between different shapes without requiring repeated, direct mechanical deformation events. Shape switching microparticles often rely on pre-alignment, or biased regions of mismatched properties, to achieve shape changes upon application of a stimulus.[10–12] A common method to generate shape switching particles is to embed them in a film and strain that film, which deforms the particles. Such a strain is often followed by a secondary programming process, possibly involving additional reactions, to stabilize this shape.[10,13,14] Although this method is effective for achieving shape switching particles, harvesting the programmed particles for desired application involves additional steps to embed particles in a matrix and subsequently remove the matrix and recover the programmed particles.

Recently, the unique optical and phase changing properties of liquid crystals (LCs) have been integrated into liquid crystal microparticle (LCMP) systems.[15–18] LCMPs demonstrating two-way shape switching behavior have been investigated, but the fabrication methods have challenges in scalability, or generate nanoparticles with size-limitations.[19–22] Some demonstrations of two-way shape switching liquid crystal elastomer microparticles (LCEMPs) use radical based polymerizations mediated by microfluidic set-ups to generate particles with pre-alignment of the LC mesogens, enabling inherent shape switching capabilities.[16,23,24] In LCEMPs, a physical pre-alignment of mesogens tethered to a polymer network define one of two accessible particle geometries. When the particles are heated past their nematic–isotropic phase transition temperature ($T_{NI}$), the polymer network contracts parallel to the alignment director and expands perpendicular to the alignment director, thus accessing the second geometry.

[a] *Department of Materials Science and Engineering, University of Colorado Boulder, 596 UCB, Boulder, CO 80309, USA. E-mail: christopher.bowman@colorado.edu*
[b] *Department of Mechanical Engineering, Montana State University, Culbertson Hall, 100, Bozeman, MT 59717, USA*
[c] *Applied Chemicals and Materials Division, National Institute of Standards and Technology, 325 Broadway, Boulder, CO 80305, USA*
[d] *Department of Chemical and Biological Engineering, University of Colorado Boulder, 596 UCB, Boulder, CO 80309, USA*

† Electronic supplementary information (ESI) available. See DOI: 10.1039/d0sm01836h

Temperature modulation enables repeated switching between geometries, resulting in a two-way shape switching capable material.[25,26] These LCEMPs are crosslinked materials, yet microfluidic systems have challenges with regard to scaling up. Recently, Schenning and coworkers reported a facile dispersion polymerization method to generate scalable, programmable LCEMPs.[10] Their method utilizes a thiol-Michael dispersion polymerization, which eliminates the need for microfluidic equipment or the oxygen controlled environments radical based polymerizations require.[27–29] To program these LCEMPs, Schenning and coworkers deform the particles embedded in a film, aligning the LC mesogens into a new prolate or oblate particle shape. Next, they use a second stage polymerization to alter the chemical composition, thus permanently crosslinking these particles into the deformed shape below the $T_{NI}$, an approach which has previously been demonstrated in bulk liquid crystal elastomers (LCEs).[26] Temporary recovery of the original spherical shape is achieved by heating past the $T_{NI}$. This system is the most viable approach to a scalable system achieving switchable particle geometries but requires particle crosslink density to be permanently altered during shape programming, which lacks a capacity for re-programmability.

Reported here is a facile means to generate and program LCEMPs comprised of a covalent adaptable network (CAN) into permanent or reprogrammable shapes, achieving two-way shape switching capabilities. By employing a CAN, a typical static polymer network is rendered dynamic upon application of the appropriate stimulus.[30,31] The dynamic network acts to relieve stress, imparted through a straining event, by reconfiguring the network and allowing it to trend towards a thermodynamic equilibrium through exchangeable crosslinks. A variety of stimuli exist for network reconfiguration of CAN-based LCE materials, including thermal activation of vitrimers; however, in the work reported here, light activation is used to decouple the thermotropic LC phase transition from the programming stimulus.[32,33] A reversibly programmable and two-way shape switching mechanism has been demonstrated in a light activated CAN-based bulk LCE, as reported by McBride *et al.*, but this mechanism has not previously been demonstrated in micron-scale LC particles.[34] Furthermore, Non-LC CAN-based particles have been reported that do not switch shape, unlike the system reported here that has two-way shape switching capabilities due to the LCE character of the particles.[35] Reported here, a thiol-Michael dispersion polymerization is used to generate CAN-based LCEMPs, which alleviates the aforementioned challenges of scale-up and oxygen sensitivity identified in microfluidic and radical-based precipitation polymerizations. The CAN mechanism utilized is mediated by a light initiated addition–fragmentation chain-transfer (AFT) reaction, where the crosslink density of the network remains unchanged throughout the duration of the programming steps following polymerization.[30,31] Once AFT-LCEMPs are programmed to a new shape, the original spherical shape of the particle is recovered and/or further altered in subsequent programming steps, limited only by the amount of photoinitiator available in the system. Particles were also programmed to have a complex surface topography.

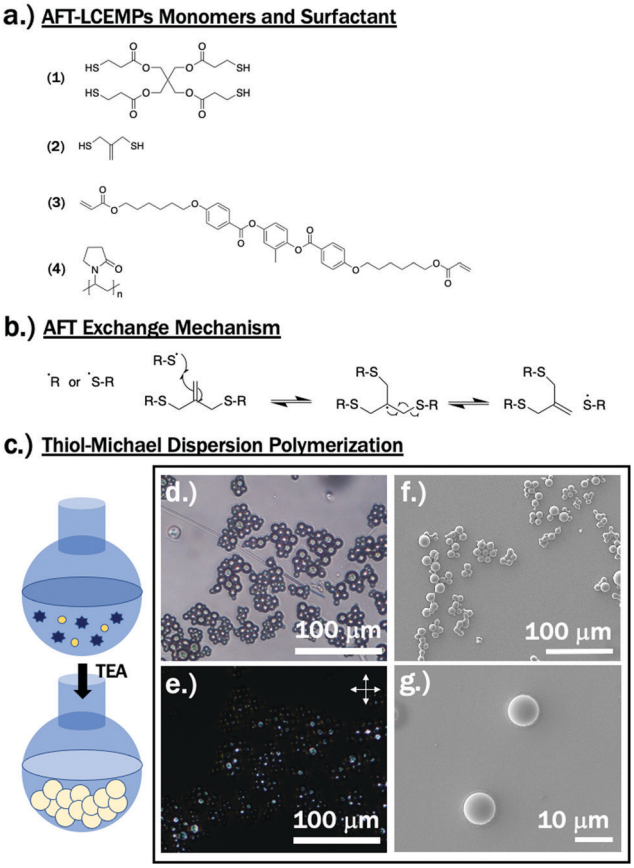


Fig. 1 (a) Monomers and surfactant for the thiol-Michael dispersion polymerization (1) PETMP, (2) ADT the AFT moiety, (3) RM82, (4) PVP surfactant (b) AFT exchange mechanism. Crosslink density is maintained due to the exchange type mechanism where a radical adds into the exchangeable moiety before a sulfide bond is broken. (c) Thiol-Michael dispersion polymerization scheme with catalyst TEA added to start the reaction. AFT-LCEMPs as polymerized, (d) optical microscopy, (e) polarized optical microscopy (f and g) SEM.

The AFT-LCEMPs reported here were generated by thiol-Michael dispersion polymerization. The monomers used to generate the AFT-LCEMPs include the following: a polymerizable diacrylate liquid crystal RM82, a tetra-thiol crosslinker pentaerythritol tetrakis(3-mercaptopropionate) (PETMP), an exchangeable moiety the allyl dithiol (ADT), and the surfactant polyvinylpyrrolidone (PVP) (Fig. 1a). The AFT exchange reaction chosen requires an exchangeable moiety, in this system, the allyl sulfide functionality that is achieved by the ADT monomer. By embedding this exchangeable moiety in the network backbone, the covalent crosslinks are altered from static to dynamic upon photoinitiation of a radical species, which generates a cascading bond exchange reaction facilitated by the allyl sulfide functionality of the exchangeable moiety during light exposure to relieve stress in the network, while maintaining the crosslink density during the exchange reaction (Fig. 1b).[30,31] The monomers were added to a MeOH/DCM mixture, with a slight excess of the thiol crosslinker, in the following monomer molar ratios; PETMP : ADT : RM82 1.05 : 2 : 4. A slight excess of the thiol crosslinker was used to increase the acrylate conversion so as to eliminate acrylate polymerization in the second step, which requires

 

light initiation of a radical species to start the bond exchange reaction for shape programming. Secondary acrylate polymerizations are used in dual cure methods from aforementioned programming techniques, but here the reaction mechanism for programming relies on covalent bond exchange instead of a secondary polymerization. PVP was used to stabilize microparticle formation and finally, triethylamine (TEA) was added to catalyze the thiol-Michael reaction, which was allowed to run overnight (Fig. 1c).

This polymerization yielded AFT-LCEMPs with an average diameter ($D_n$) of 7 μm ± 2 μm and a coefficient of variance (CV) of 31%, as calculated by eqn (1),

$$\mathrm{CV}\% = \frac{\mathrm{SD}}{D_n} \times 100 \quad (1)$$

where the standard deviation (SD) is divided by $D_n$. Particle size distribution is reported in further detail by the bar graph included in Fig. S1 (ESI†). A glass transition ($T_g$) of −8.5 °C was determined by differential scanning calorimetry (DSC) on dried particles, indicating that the material is rubbery at room temperature and well-suited for manual deformation (Fig. S2, ESI†). DSC also indicated a $T_{NI}$ of 115 °C. After the polymerization was complete, the particles were washed and observed under optical microscopy (OM) and polarized optical microscopy (POM), displaying the characteristic birefringence of polydomain LC alignment (Fig. 1d and e). Scanning electron microscopy (SEM) was also performed on the as-polymerized particles, seen in Fig. 1f and g. The AFT-LCEMPs were then programmed to have two-way shape switching capabilities.

To program the two-way shape switching of the AFT-LCEMPs, particles were processed following the programming scheme seen in Fig. 2a. First, particles were deposited on a glass slide and compressed manually by a second piece of glass (superstrate) at room temperature, resulting in a prolate shape (Fig. 2b and Fig. S3, ESI†). This shape is often seen in actuatable LCEMPs due to the directed re-orientation of LC mesogens by the deformation mechanism.[10,16] Observed in the corresponding POM images is the change in birefringence from spherical particles, exhibiting a consistent blue hue (Fig. 1e),

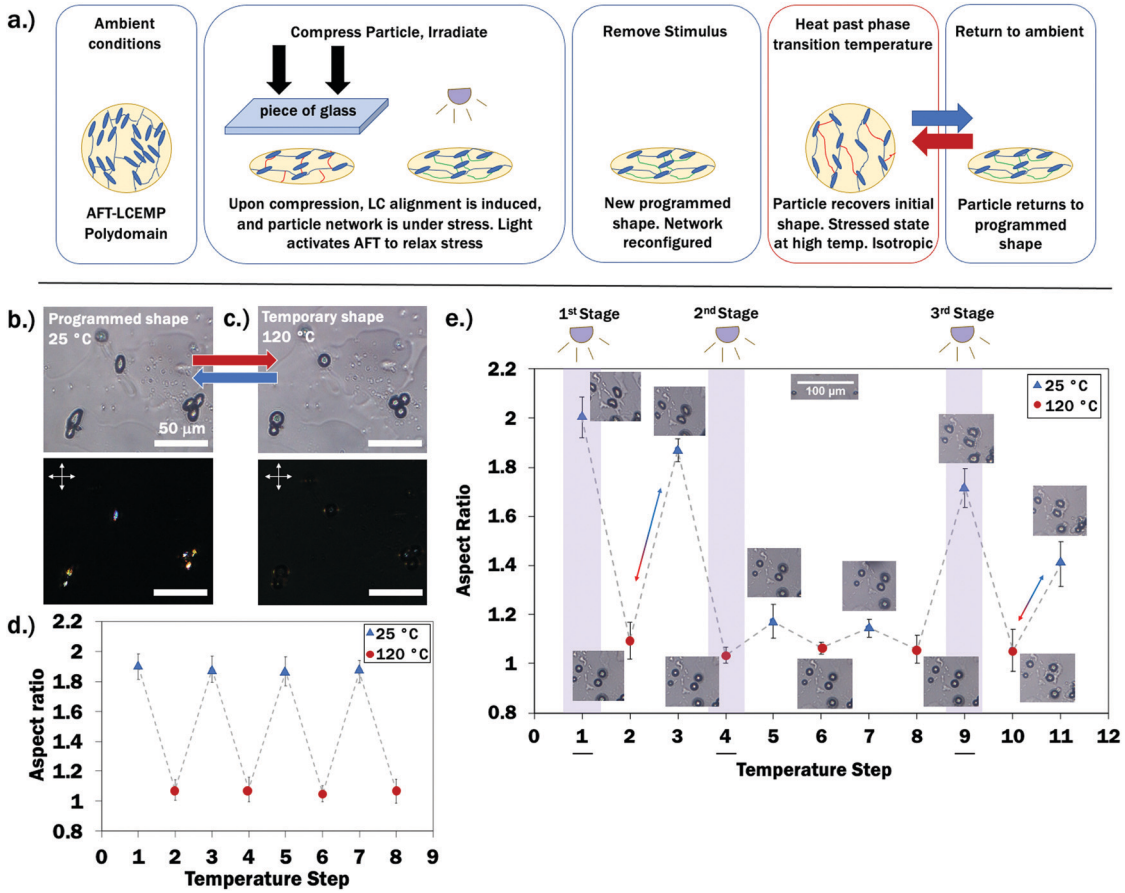


Fig. 2 (a) Schematic of programming particles and shape switching behavior of particles after programming. (b) Particles after programming displaying a prolate shape at room temperature (top) OM (bottom) POM. (c) Particles at 120 °C recovering their temporary spherical shape and appearing almost fully isotropic in POM with birefringence almost completely gone. (d) Aspect ratio plot for particles undergoing temperature cycles and switching shape from prolate to spherical. Dashed line for ease of viewing. (e) Aspect ratio plot of particles undergoing three programming steps: 1st Stage – Particles pictured after compression and irradiated with light, programmed to the prolate shape at Temp. Step 1. Particles cycle shape between Temp. Step 2 and 3. 2nd Stage – particles undergo a re-programming step, light exposure at high temperature, back to the spherical shape at Temp. Step 4. 3rd Stage – particles undergo a final programming step, particles pictured after compression and irradiated with light, programmed back to the prolate shape at Temp. Step 9. Particles cycle shape between Temp. Step 10 and 11. Dashed line for ease of viewing.

to the prolate shaped particles, exhibiting significant variation of color (Fig. 2b and Fig. S4a, ESI†), indicating the change in LC alignment associated with the change in shape. Birefringence disappears as prolate particles are angled 45 degrees to the cross-polarizers, indicating a skewed alignment along the long axis of the particle, with some remaining birefringence seen near the tips where alignment is constrained by particle geometry (Fig. S4b, ESI†). There are several factors which may contribute to the deformed particle shape including crosslink density, particle size, and LC phase that are not systematically explored here and remain open questions regarding the degrees of control afforded by these AFT-LCEMPs.

Next, the glass used for compression was removed and the particles were found to maintain their deformed shape due to soft elasticity arising from the LC mesogen reorientation.[36] A bulk LCE analog was fabricated to generate a stress–strain profile representative of the particle material properties (Fig. S5, ESI†). The soft elasticity is exhibited by the decrease in stress starting at about 35% strain, indicative of the LC mesogen reorientation. It is also important to note that the stress–strain profile for a spherical particle might be somewhat altered due to shape confinement in contrast to the rectangularly shaped bulk LCE analog used for analysis. The AFT reaction acts to relieve stress on the crosslinks generated from the strain deformation event, which in this study is compression of the particle network. Compression at room temperature shifts the polydomain LC mesogen alignment towards a global alignment, yielding the observed prolate particle shape.

After compression, the sample is irradiated with low wavelength light, used to initiate the AFT exchange reaction *via* the photoinitiator 2,2-dimethoxy-2-phenylacetophenone (DMPA) and/or Irgacure 819 as indicated in the ESI,† which are swollen into the particle after polymerization. Two initiators with different absorbance profiles were used to increase the amount of accessible initiator for programming cycles. The bond exchange facilitated by AFT relaxes the stresses applied to the particle, and this new LC alignment is stabilized without altering the crosslink density due to the exchange-based relaxation mechanism.[30,31] Using light to initiate the exchange reaction decouples this programming step from the temperature dependent LC phase behavior of the particles, giving control over the conditions under which programming and actuation occur. Following this programming step, the particles were heated past their $T_{NI}$ of 115 °C to 120 °C, and the original spherical shape was recovered (Fig. 2c and Fig. S6b, ESI†). A near-isotropic phase is confirmed by corresponding POM images with nearly complete absence of birefringence. Due to the programmed LC alignment at room temperature in the LC phase, as the particles move through their LC phase transition to the isotropic phase, they experience a contraction parallel to the aligned director, and expansion perpendicular to the director, returning them to a spherical shape, which is characteristic of shape changing LCEs.[25,34] Upon cooling back to the LC phase at room temperature, the particles return to their prolate programmed shape (Fig. 2b and Fig. S6a, ESI†).

Thermally cycling the programmed particles reliably cycles the particles through a prolate shape in the low-temperature LC phase to a spherical shape in the high-temperature isotropic phase (Fig. 2b and c), as quantified by the aspect ratio. Aspect ratio, or the ratio of an objects' length to its width, was measured from OM using ImageJ to analyze the change in shape from the prolate shape in the LC phase to the spherical shape in the isotropic phase, upon thermally cycling the particles multiple times after programming (Fig. 2d). The aspect ratio was calculated using the following equation:

$$A_R = \frac{d_2}{d_1} \quad (2)$$

where $d_1$ represents the particle short axis and $d_2$ represents the particle long axis.[20] After programming and thermal cycling, the particles measured in the LC phase achieved an average aspect ratio of 1.89 with 90 ± 4% shape fixity, which describes the relatively high aspect ratio of the prolate shape observed in OM and SEM. Particles measured in the isotropic phase displayed an average aspect ratio of 1.1 with 95 ± 4% shape recovery from an un-programmed spherical particle, corresponding to the spherical shape they temporarily exhibit. In comparison, initially polymerized un-programmed particles exhibit an average aspect ratio of 1.

A variety of control experiments were performed to establish that AFT programming in this study relies on the presence of the AFT moiety, and photoinitiator coupled with light exposure to activate the exchange. In the first control, AFT-LCEMPs were not swollen with photoinitiator, but were still compressed to a prolate shape, irradiated with light, and thermally cycled past the $T_{NI}$. These AFT-LCEMPs returned to their initial spherical shape with the aspect ratio returning to 1, demonstrating the need for photoinitiator to program the prolate shape (Fig. S7a and b, ESI†). In parallel, non-AFT capable LCEMPs were swollen with photoinitiator, compressed to the prolate shape, irradiated with light, and thermally cycled past the $T_{NI}$, again returning to their initial spherical shape with an aspect ratio of 1, demonstrating the need for the AFT moiety (Fig. S7c and d, ESI†). In an additional control, no light exposure and no photoinitiator were used, but the particles were compressed to the prolate shape and thermally cycled past the $T_{NI}$, returning to their initial spherical shape, both returning to an aspect ratio of 1, demonstrating the need of photoinitiator coupled with light exposure for programming (Fig. S8a–d, ESI†). Shape recovery back to an aspect ratio of 1 eliminates the possibility of substrate adhesion being an issue for prolate to spherical shape recovery on glass substrates. All controls, regardless of initiator content, were pre-irradiated with light to ensure any excess acrylate and thiol were reacted and thus controls were started under the same conditions (Fig. S9, ESI†).

To demonstrate the re-programmability of the AFT-LCEMPs, a 3-stage programming series was performed. Particles underwent the same programming procedure described above to achieve the reversible prolate-to-spherical shape switching, designated by the 1st Stage at temperature Step 1 of Fig. 2e. The particles pictured at Temperature Step 1 of Fig. 2e have been compressed and irradiated with light at room temperature. The programmed particles are thermally cycled past their

 

$T_{NI}$, with the corresponding particle images from Temperature Step 2 and 3 (Fig. 2e) being the new switchable prolate and spherical shapes, respectively. The prolate shape has an average aspect ratio of 1.87, with a shape fixity of 93 ± 2% from the initial compressed prolate shape.

The programmed prolate shaped particles then underwent light exposure at high temperature, to erase the prolate shape and return to a permanent spherical shape, as performed in the 2nd Stage at Temperature Step 4 (Fig. 2e and Fig. S10, ESI†). In the 1st Stage, programming to the prolate shape, the network was reconfigured such that it is in a nearly stress-free thermodynamic equilibrium at room temperature. Upon heating past the LC phase transition to 120 °C, the movement of LC mesogens and polymer chains back to an entropically driven sphere puts stress on the reconfigured network. The particles at high temperature were exposed to light to reprogram this spherical shape by allowing relaxation of the stress generated in the network at high temperature. Upon cooling back to room temperature, the particles maintained the spherical shape with an average aspect ratio of 1.1 and 88 ± 5% spherical shape recovery as compared to an initially polymerized un-programmed spherical particle, displayed at Temperature Steps 5 and 7 (Fig. 2e). Cooling and heating cycles shown at Temperature Steps 4 through 8 (Fig. 2e) demonstrate significant recovery of the spherical shape after stress relaxation, although not 100%, which is attributed to insufficient stress relaxation to completely erase the prolate shape, resulting from either the depletion of the necessary photoinitiator or insufficient light exposure.

To demonstrate one more programming iteration, the re-programmed spherical particles underwent a final programming event, back to a prolate shape, by manual compression and light irradiation at room temperature, performed in the 3rd Stage at Temperature Step 9 (Fig. 2e and Fig. S11, ESI†). After thermal cycling past the $T_{NI}$, displayed at Temperature Step 11 (Fig. 2e), the particles exhibited an average aspect ratio of 1.4, with 82 ± 2% shape fixity from the initially compressed prolate shape at Temperature Step 9 (Fig. 2e). This new prolate shape consistently cycles shape between the aspect ratios recorded at Temperature Steps 10 and 11 (Fig. 2e).

Variables contributing to the programmability of the particles include photoinitiator concentration, achievable applied strain, temperature, and duration of light exposure, which were not systematically studied here. This behavior has been studied in bulk AFT-LCEs reported by McBride *et al.*, and little deviation from that qualitative behavior would be expected in these microparticles.[34] The strain applied to the particles varied from 20 to 40% strain, a result of particle size polydispersity, so the fixity is reported for the particles from their initial deformed shape to their new permanent shape after thermally cycling, with an effort to analyze particles of similar sizes and strains. About 67 ± 1% of particles casted were successfully deformed and programmed, while 32 ± 3% remained un-deformed and un-programmed due to lack of contact with the superstrate, with these particles being 4 microns or smaller. There was no noticeable threshold on size dependence for shape switching capabilities, with the limiting factor being particle contact with the superstrate to result in deformation.

To access more particle geometries, AFT-LCEMPs were programmed by nanoimprint lithography (NIL). NIL allows for controlled heating and light irradiation during compression. NIL was used to achieve a permanent oblate shape configuration. Particles swollen with photoinitiator were deposited on silicon, heated past their $T_{NI}$ to 140 °C, and subjected to compression with a flat glass superstrate at this high temperature, yielding an oblate shape. The particles being in their isotropic phase, now deform into an oblate shape with LC mesogens and polymer chains having more mobility to deform at high temperature. The particles were exposed to light at high temperature under compression to activate the AFT bond exchange and were then cooled to ambient, achieving a permanent oblate shape (Fig. 3a). Atomic Force Microscopy (AFM) was done to confirm the height profile and aspect ratio of the particles, with a 15 : 3 length to height ratio (Fig. 3b).

Furthering the application possibilities of AFT-LCEMPs for photonics or rheological control, particles were programmed to have a switchable complex surface topography, aided by the AFT exchange. The particle surface was patterned with a line grating by NIL, substituting the flat superstrate for one with a diffraction grating of 833 nm periodicity. Undergoing compression at 140 °C during light exposure, with 5-micron spacers dispersed on the substrate surface to control compression, the particles yield a line-patterned surface topography at high temperature, as determined by AFM (Fig. 4a). AFM of a particle cross-section indicates that the imprinting yields about 150 ± 60 nm deep surface features, which is about 75% of the depth of the 200 nm deep grooves in the mold (Fig. S12, ESI†). Due to the curved particle shape, the average pattern depth was calculated from measurements taken towards the center of the particle surface. Upon cooling below the $T_{NI}$ to 35 °C, the

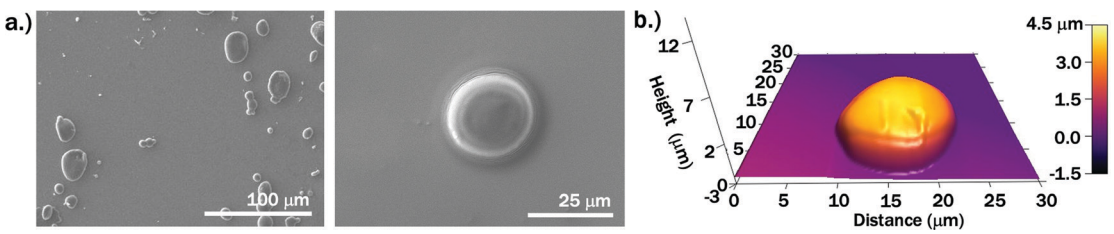


Fig. 3 (a) SEM of particles after undergoing NIL, run with a flat superstrate under compression at 140 °C to program a permanent oblate shape. (b) AFM of an oblate programmed particle displaying the flat particle aspect ratio of 15 : 3 length to height ratio.

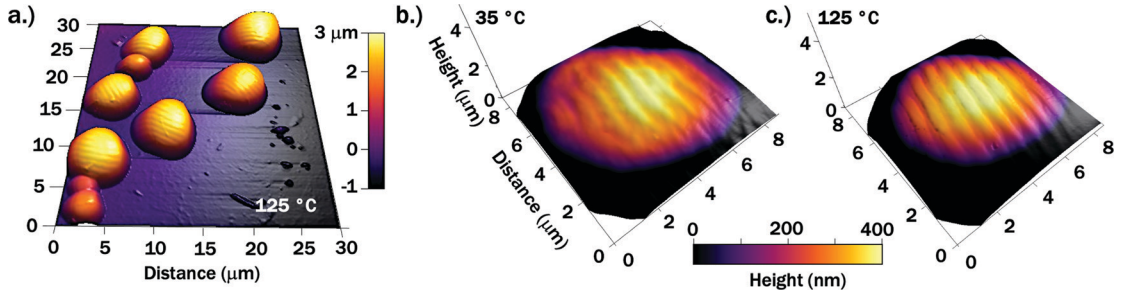


Fig. 4 (a) AFM of multiple particles imaged at 125 °C displaying the patterned surface topography incurred by NIL programming, compressed at 140 °C using a diffraction grating mold as the superstrate. (b) AFM of a particle surface imaged at 35 °C displaying pattern disruption. (c) AFM of the same particle surface imaged at 125 °C displaying pattern recovery. Axes for (b and c) are in μm as indicated by (b).

patterned surface is disrupted (Fig. 4b). Heating the particles above the $T_{NI}$ recovers the imprinted pattern, creating a switchable complex surface (Fig. 4c). Alternately, imprinting done without spacers yields a complex surface topography below the $T_{NI}$ (Fig. S13, ESI†). NIL has been studied on AFT capable materials, specifically on bulk AFT-LCEs as reported by McBride *et al.*, and separately on non-LC AFT-particles as reported by Cox *et al.*, but has not been reported for AFT-LCEMPs before.[34,35] Influences which may contribute to controlling the surface topography are material properties including particle size and shape, chemical composition, temperature, irradiation, and applied strain. Complex surface topography of microparticles often occurs during polymerization, modulated by polymerization conditions, monomer content, or deswelling, whereas in this study, the surface topography is modified post-polymerization at the users' discretion.[17,37,38] These complex surface topographies are advantageous for photonics and controlling surface adhesion or rheological behavior.

## Conclusions

Reported here is a facile and scalable means to achieve reversibly programmable AFT-LCEMPs *via* a thiol-Michael dispersion polymerization. Undergoing a light-initiated programming event, the particles were programmed to be two-way shape switching capable by irradiating particles that had been compressed into a prolate shape with light to initiate AFT bond exchange. This exchange relieved stress in the network to achieve a low temperature prolate shape. Upon heating and cooling, these particles cyclically transitioned between spherical and prolate, respectively. Furthermore, these two-way shape switching particles were shown to be reversibly programmable by irradiating the particles at high temperature, while in their temporary spherical shape, to return them to their original permanent spherical shape. The particles were also programmed to achieve a permanent oblate shape, and separately, the surface was programmed with a switchable diffraction grating, demonstrating control over the surface topography. The particles are reusable due to their AFT re-programmability and can be re-swollen with photoinitiator to facilitate additional programming events. These AFT-LCEMPs have potential applications in micro-actuation, photonics, or surface control, which can be made adaptable at the users' discretion.

## Conflicts of interest

There are no known conflicts of interest.

## Acknowledgements

This work was completed with the financial support of NSF DMR 1809841 and NIH grant 1 F31 DE027861-01A1. The authors gratefully acknowledge Professor Timothy White's lab, Tayler Hebner, and Kyle Schlafmann, for use of their DSC at the University of Colorado, Boulder. The authors gratefully acknowledge Professor Yifu Ding's lab and Adrienne Blevins, for use of their nanoimprinter at the University of Colorado, Boulder. The authors gratefully acknowledge the COSINC-CHR facility and Dr Tomoko Borsa, for use of the FESEM at the University of Colorado, Boulder. Certain commercial equipment, instruments, or materials are identified in this paper in order to specify the experimental procedure adequately. Such identification is not intended to imply recommendation or endorsement by NIST. Contribution of NIST, an agency of the U.S. government; not subject to copyright.

## References

1 V. B. Patravale and S. D. Mandawgade, Novel Cosmetic Delivery Systems: An Application Update: Novel Cosmetic Delivery Systems, *Int. J. Cosmetic Sci.*, 2008, **30**(1), 19–33, DOI: 10.1111/j.1468-2494.2008.00416.x.

2 D. T. Birnbaum and L. Brannon-Peppas, Microparticle Drug Delivery Systems, in *Drug Delivery Systems in Cancer Therapy*, ed. D. M. Brown, Humana Press, Totowa, NJ, 2004, pp. 117–135, DOI: 10.1007/978-1-59259-427-6_6.

3 Y. Xia, B. Gates, Y. Yin and Y. Lu, Monodispersed Colloidal Spheres: Old Materials with New Applications, *Adv. Mater.*, 2000, **12**(10), 693–713, DOI: 10.1002/(SICI)1521-4095(200005)12:10⟨693::AID-ADMA693⟩3.0.CO;2-J.

4 H. P. C. van Kuringen, D. J. Mulder, E. Beltran, D. J. Broer and A. P. H. J. Schenning, Nanoporous Polymer Particles Made by Suspension Polymerization: Spontaneous Symmetry Breaking

 

in Hydrogen Bonded Smectic Liquid Crystalline Droplets and High Adsorption Characteristics, *Polym. Chem.*, 2016, **7**(29), 4712–4716, DOI: 10.1039/C6PY00865H.

5 S. Bhaskar, K. M. Pollock, M. Yoshida and J. Lahann, Towards Designer Microparticles: Simultaneous Control of Anisotropy, Shape, and Size, *Small*, 2010, **6**(3), 404–411, DOI: 10.1002/smll.200901306.

6 L. M. Cox, J. P. Killgore, Z. Li, R. Long, A. W. Sanders, J. Xiao and Y. Ding, Influences of Substrate Adhesion and Particle Size on the Shape Memory Effect of Polystyrene Particles, *Langmuir*, 2016, **32**(15), 3691–3698, DOI: 10.1021/acs.langmuir.6b00588.

7 S. Mueller, E. W. Llewellin and H. M. Mader, The Rheology of Suspensions of Solid Particles, *Proc. R. Soc. A*, 2010, **466**(2116), 1201–1228, DOI: 10.1098/rspa.2009.0445.

8 K. Uto and M. Ebara, Magnetic-Responsive Microparticles That Switch Shape at 37 °C, *Appl. Sci.*, 2017, **7**(11), 1203, DOI: 10.3390/app7111203.

9 J. E. Marshall, S. Gallagher, E. M. Terentjev and S. K. Smoukov, Anisotropic Colloidal Micromuscles from Liquid Crystal Elastomers, *J. Am. Chem. Soc.*, 2014, **136**(1), 474–479, DOI: 10.1021/ja410930g.

10 X. Liu, X. Pan, M. Debije, J. Huets, D. Mulder and A. Schenning, Programmable Liquid Crystal Elastomer Microactuators Prepared via Thiol-Ene Dispersion Polymerization, *Soft Matter*, 2020, **13**(45), 8368–8378, DOI: 10.1039/C7SM01619K.

11 D. Klinger, C. X. Wang, L. A. Connal, D. J. Audus, S. G. Jang, S. Kraemer, K. L. Killops, G. H. Fredrickson, E. J. Kramer and C. J. Hawker, A Facile Synthesis of Dynamic, Shape-Changing Polymer Particles, *Angew. Chem., Int. Ed.*, 2014, **53**(27), 7018–7022, DOI: 10.1002/anie.201400183.

12 C. Wischke, M. Schossig and A. Lendlein, Shape-Memory Effect of Micro-/Nanoparticles from Thermoplastic Multiblock Copolymers, *Small*, 2014, **10**(1), 83–87, DOI: 10.1002/smll.201202213.

13 C. C. Ho, A. Keller, J. A. Odell and R. H. Ottewill, Preparation of Monodisperse Ellipsoidal Polystyrene Particles, *Colloid Polym. Sci.*, 1993, **271**(5), 469–479, DOI: 10.1007/BF00657391.

14 A. Rešetič, J. Milavec, B. Zupančič, V. Domenici and B. Zalar, Polymer-Dispersed Liquid Crystal Elastomers, *Nat. Commun.*, 2016, **7**, 13140, DOI: 10.1038/ncomms13140.

15 A. Belmonte, T. Bus, D. J. Broer and A. P. H. J. Schenning, Patterned Full-Color Reflective Coatings Based on Photonic Cholesteric Liquid-Crystalline Particles, *ACS Appl. Mater. Interfaces*, 2019, **11**(15), 14376–14382, DOI: 10.1021/acsami.9b02680.

16 C. Ohm, C. Serra and R. Zentel, A Continuous Flow Synthesis of Micrometer-Sized Actuators from Liquid Crystalline Elastomers, *Adv. Mater.*, 2009, **21**(47), 4859–4862, DOI: 10.1002/adma.200901522.

17 H. Yu, H. Liu and T. Kobayashi, Fabrication and Photoresponse of Supramolecular Liquid−Crystalline Microparticles, *ACS Appl. Mater. Interfaces*, 2011, **3**(4), 1333–1340, DOI: 10.1021/am2001289.

18 A. Ryabchun and A. Bobrovsky, Photocontrollable Deformations of Polymer Particles in Elastic Matrix, *Adv. Opt. Mater.*, 2019, **7**(24), 1901486, DOI: 10.1002/adom.201901486.

19 M. Vennes and R. Zentel, Liquid-Crystalline Colloidal Particles, *Macromol. Chem. Phys.*, 2004, **205**(17), 2303–2311, DOI: 10.1002/macp.200400296.

20 Z. Yang, W. T. S. Huck, S. M. Clarke, A. R. Tajbakhsh and E. M. Terentjev, Shape-Memory Nanoparticles from Inherently Non-Spherical Polymer Colloids, *Nat. Mater.*, 2005, **4**(6), 486–490, DOI: 10.1038/nmat1389.

21 S. Haseloh, C. Ohm, F. Smallwood and R. Zentel, Nanosized Shape-Changing Colloids from Liquid Crystalline Elastomers, *Macromol. Rapid Commun.*, 2011, **32**(1), 88–93, DOI: 10.1002/marc.201000324.

22 S. Haseloh and R. Zentel, Synthesis of Liquid-Crystalline Colloids in Nonpolar Media and Their Manipulation in Electric Fields, *Macromol. Chem. Phys.*, 2009, **210**(17), 1394–1401, DOI: 10.1002/macp.200900122.

23 T. Hessberger, L. Braun and R. Zentel, Microfluidic Synthesis of Actuating Microparticles from a Thiol-Ene Based Main-Chain Liquid Crystalline Elastomer, *Polymers*, 2016, **8**(12), 410, DOI: 10.3390/polym8120410.

24 E.-K. Fleischmann, F. R. Forst, K. Köder, N. Kapernaum and R. Zentel, Microactuators from a Main-Chain Liquid Crystalline Elastomer via Thiol–Ene ''Click'' Chemistry, *J. Mater. Chem. C*, 2013, **1**(37), 5885, DOI: 10.1039/c3tc30272e.

25 T. J. White and D. J. Broer, Programmable and Adaptive Mechanics with Liquid Crystal Polymer Networks and Elastomers, *Nat. Mater.*, 2015, **14**(11), 1087–1098, DOI: 10.1038/nmat4433.

26 C. M. Yakacki, M. Saed, D. P. Nair, T. Gong, S. M. Reed and C. N. Bowman, Tailorable and Programmable Liquid-Crystalline Elastomers Using a Two-Stage Thiol–Acrylate Reaction, *RSC Adv.*, 2015, **5**(25), 18997–19001, DOI: 10.1039/C5RA01039J.

27 X. Liu, Y. Xu, J. P. A. Heuts, M. G. Debije and A. P. H. J. Schenning, Monodisperse Liquid Crystal Network Particles Synthesized via Precipitation Polymerization, *Macromolecules*, 2019, **52**(21), 8339–8345, DOI: 10.1021/acs.macromol.9b01852.

28 C. Wang, X. Zhang, M. Podgórski, W. Xi, P. Shah, J. Stansbury and C. N. Bowman, Monodispersity/Narrow Polydispersity Cross-Linked Microparticles Prepared by Step-Growth Thiol–Michael Addition Dispersion Polymerizations, *Macromolecules*, 2015, **48**(23), 8461–8470, DOI: 10.1021/acs.macromol.5b02146.

29 O. Z. Durham and D. A. Shipp, Polymer Colloids from Step-Growth Thiol-X Polymerizations, *Polym. Rev.*, 2020, 1–26, DOI: 10.1080/15583724.2020.1743307.

30 M. K. McBride, B. T. Worrell, T. Brown, L. M. Cox, N. Sowan, C. Wang, M. Podgorski, A. M. Martinez and C. N. Bowman, Enabling Applications of Covalent Adaptable Networks, *Annu. Rev. Chem. Biomol. Eng.*, 2019, **10**(1), 175–198, DOI: 10.1146/annurev-chembioeng-060718-030217.

31 C. J. Kloxin, T. F. Scott, B. J. Adzima and C. N. Bowman, Covalent Adaptable Networks (CANs): A Unique Paradigm in Cross-Linked Polymers, *Macromolecules*, 2010, **43**(6), 2643–2653, DOI: 10.1021/ma902596s.

32 D. W. Hanzon, N. A. Traugutt, M. K. McBride, C. N. Bowman, C. M. Yakacki and K. Yu, Adaptable Liquid

Crystal Elastomers with Transesterification-Based Bond Exchange Reactions, *Soft Matter*, 2018, **14**(6), 951–960, DOI: 10.1039/C7SM02110K.

33 M. O. Saed, A. Gablier and E. M. Terentejv, Liquid Crystalline Vitrimers with Full or Partial Boronic-Ester Bond Exchange, *Adv. Funct. Mater.*, 2020, **30**(3), 1906458, DOI: 10.1002/adfm.201906458.

34 M. K. McBride, A. M. Martinez, L. Cox, M. Alim, K. Childress, M. Beiswinger, M. Podgorski, B. T. Worrell, J. Killgore and C. N. Bowman, A Readily Programmable, Fully Reversible Shape-Switching Material, *Sci. Adv.*, 2018, **4**(8), eaat4634, DOI: 10.1126/sciadv.aat4634.

35 L. M. Cox, X. Sun, C. Wang, N. Sowan, J. P. Killgore, R. Long, H.-A. Wu, C. N. Bowman and Y. Ding, Light-Stimulated Permanent Shape Reconfiguration in Cross-Linked Polymer Microparticles, *ACS Appl. Mater. Interfaces*, 2017, **9**(16), 14422–14428, DOI: 10.1021/acsami.7b02759.

36 T. H. Ware, J. S. Biggins, A. F. Shick, M. Warner and T. J. White, Localized Soft Elasticity in Liquid Crystal Elastomers, *Nat. Commun.*, 2016, **7**, 10781, DOI: 10.1038/ncomms10781.

37 H. Yu, C. Dong, W. Zhou, T. Kobayashi and H. Yang, Wrinkled Liquid-Crystalline Microparticle-Enhanced Photoresponse of PDLC-Like Films by Coupling with Mechanical Stretching, *Small*, 2011, **7**(21), 3039–3045, DOI: 10.1002/smll.201101098.

38 J. Liu, Y. Liu, Y. Xue, Y. Ren, X. Fan, R. Wang, H. Zhang, B. Zhang and Q. Zhang, Fabrication and Characterization of Controllable Wrinkled-Surface Polymer Microparticles, *J. Mater. Sci.*, 2019, **54**(7), 5852–5864, DOI: 10.1007/s10853-018-2421-2.

 